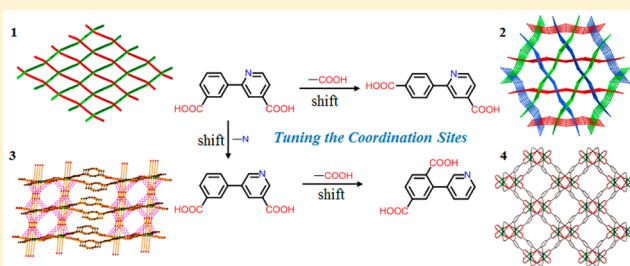


Structural Diversity of Cadmium(II) Coordination Polymers Induced by Tuning the Coordination Sites of Isomeric Ligands

Bo Liu,^{†,‡} Hui-Fang Zhou,[‡] Lei Hou,^{*,‡} Jian-Ping Wang,[†] Yao-Yu Wang,[‡] and Zhonghua Zhu[§][†]College of Science, Northwest A&F University, Yangling 712100, People's Republic of China[‡]Key Laboratory of Synthetic and Natural Functional Molecule Chemistry of the Ministry of Education, College of Chemistry & Materials Science, Northwest University, Xi'an 710069, People's Republic of China[§]School of Chemical Engineering, The University of Queensland, Brisbane 4072, Australia

Supporting Information

ABSTRACT: When the coordination sites of ligands were shifted, the solvothermal reactions of four positional isomeric asymmetrical pyridyldicarboxylic acids with $\text{Cd}(\text{NO}_3)_2$ generated four new coordination polymers, $[\text{Cd}(\text{L1})\text{-(DMF)}_3]\cdot\text{DMF}\cdot\text{H}_2\text{O}$ (1), $[\text{H}_2\text{N}(\text{CH}_3)_2][\text{Cd}(\text{L2})_2]\cdot 3\text{DMF}\cdot\text{H}_2\text{O}$ (2), $[\text{Cd}(\text{L3})(\text{H}_2\text{O})_2]$ (3), and $[\text{Cd}(\text{L4})]\cdot 1.5\text{DMF}$ (4), where DMF = *N,N*-dimethylformamide, $\text{H}_2\text{L1}$ = 2-(3'-carboxylphenyl)isonicotinic acid, $\text{H}_2\text{L2}$ = 2-(4'-carboxylphenyl)isonicotinic acid, $\text{H}_2\text{L3}$ = 5-(3'-carboxylphenyl)nicotinic acid, and $\text{H}_2\text{L4}$ = 2-(3'-pyridyl)-terephthalic acid. 1 shows a rare 2D fabric structure. 2 discloses a grid-layer structure with heterochiral helical chains and in which three sets of layers stack in different directions, affording an unprecedented $2\text{D} + 2\text{D} + 2\text{D} \rightarrow 3\text{D}$ polycatenating framework with 3D intersecting porous systems. 3 also displays a 2D layer possessing strong intralayer $\pi\cdots\pi$ interactions and interlayer hydrogen bonds. 4 contains a rare $\text{Cd}_2(\text{COO})_4$ paddle-wheel unit and forms a 3D framework with 1D open channels. The carboxyl and pyridyl groups of the positional isomeric $\text{H}_2\text{L1}$ – $\text{H}_2\text{L4}$ ligands show distinct bridging fashions, which leads to the production of versatile architectures of 1–4, and their effects on the crystal structures are discussed. 1–4 reveal solid-state photoluminescence stemming from intraligand charge transfer. 2 and 4 show high selectivity for CO_2 over CH_4 but with different CO_2 adsorption enthalpies. Grand canonical Monte Carlo simulations identified the multiple adsorption sites in 2 for CO_2 .



INTRODUCTION

Increasing interest has been focused on the design and construction of novel functional coordination polymers (CPs) because of their fascinating architectures and potential applications in the areas of luminescence,¹ gas storage/separation,² heterogeneous catalysis,³ and molecular recognition.⁴ Accordingly, numerous CPs with excellent performance were assembled by various approaches. However, it remains very challenging to control CPs with the desired structures, which significantly depend on not only synthetic factors, such as solvents, pH values, and temperatures,⁵ but also the nature of the building blocks, such as metal ions, ligands, and possible templates.⁶ From a design perspective, the ligand is the most important building block because of the fact that a large number of ligands with diverse structures and properties can be synthesized by the repertoire of synthetic chemistry. Through the design of an appropriate ligand, it is possible to tune the structures and functionality of CPs.⁷ In contrast to the fruitful research in effect from the length, flexibility, and substituent groups of organic ligands,⁸ a particular series of CP species that can be systematically tuned by the positional isomeric effect and undergo structural transformations remain largely unexplored thus far. Investigations on the positional isomeric effect have been scarcely reported in polycarboxylate or pyridyl ligand

systems⁹ or their mixed-ligand systems,¹⁰ which not only illustrate the exploration of the essential factors of positional isomeric ligands for regulating structural assembly but also provide further insight into the design of new functional crystalline materials.

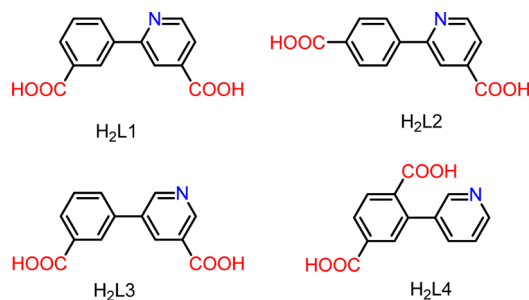
The geometry of a ligand is a crucial aspect in directing the structures of CPs. Highly symmetrical bridging polycarboxylate or pyridyl organic linkers are commonly used to prepare porous CPs, while little attention has been focused on the investigation of elongated asymmetrical pyridyldicarboxylate bridging ligands,¹¹ although these ligand-based CPs revealed unique frameworks and properties.^{11,12} In fact, the employment of low-symmetry ligands has recently been proposed as a promising synthetic strategy to construct CPs,¹³ which with increasing topological complexity offers a less-investigated direction toward CP fabrication.

Along with our recent research in the construction of CPs based on unsymmetrical pyridylcarboxylate ligands,¹⁴ with the aim of a comparative study, this work designed four asymmetrical isomeric tritopic pyridyldicarboxylic acid ligands, $\text{H}_2\text{L1}$ = 2-(3'-carboxylphenyl)isonicotinic acid, $\text{H}_2\text{L2}$ = 2-(4'-

Received: June 12, 2016

carboxylphenyl)isonicotinic acid, H₂L3 = 5-(3'-carboxylphenyl)nicotinic acid, and H₂L4 = 2-(3'-pyridyl)-terephthalic acid (Scheme 1). When these are employed with

Scheme 1. Four Positional Isomeric Pyridyldicarboxylic Acids Used in This Work



Cd²⁺ ions, four new CPs, [Cd(L1)(DMF)₃].DMF·H₂O (**1**), [H₂N(CH₃)₂]₂[Cd(L2)₂].3DMF·H₂O (**2**), [Cd(L3)(H₂O)₂] (**3**), and [Cd(L4)].1.5DMF (**4**), were prepared. **1–4** exhibit a variety of architectures from 1D chain to 2D layer to 3D framework. The carboxyl and pyridyl groups in the H₂L1–H₂L4 ligands show obviously distinct bridging fashions. The structures, luminescence, and gas-adsorption properties were investigated.

EXPERIMENTAL SECTION

Materials and General Methods. All reagents were purchased commercially and used as-received without further purification. Detailed procedures for the synthesis of H₂L1–H₂L4 are listed in Schemes S1–S4. Elemental analyses for carbon, hydrogen, and nitrogen were performed on a PerkinElmer 2400C elemental analyzer. IR spectra were recorded using KBr pellets on a Nicolet Avatar 360 Fourier transform infrared (FTIR) spectrometer. Powder X-ray diffraction (PXRD) data were collected on a Bruker D8-ADVANCE diffractometer using Cu K α radiation ($\lambda = 1.5418 \text{ \AA}$). Thermogravimetric analyses (TGA) were measured under a nitrogen stream using a heating rate of $5 \text{ }^\circ\text{C min}^{-1}$ on a Netzsch TG209F3 instrument. Gas-sorption isotherms were measured using an ASAP 2020 M adsorption instrument with an automatic volumetric sorption apparatus.

Luminescence spectra were obtained on a PerkinElmer LS55 luminescence spectrometer.

Synthesis of [Cd(L1)(DMF)₃].DMF·H₂O (1**).** A mixture of Cd(NO₃)₂·4H₂O (30.8 mg, 0.1 mmol), H₂L1 (24.3 mg, 0.1 mmol), and 2 drops of HNO₃ (0.1 M) in DMF (5 mL) was sealed in a 10 mL screw-capped vial. The vial was placed in an oven at 105 °C for 72 h and gradually cooled to room temperature at a rate of $5 \text{ }^\circ\text{C min}^{-1}$. Colorless rod crystals of **1** were collected by filtration and washed with DMF. The yield was ca. 29.8 mg (44.9%, based on H₂L1). Anal. Calcd for C₂₅H₃₇CdN₅O₉: C, 45.22; H, 5.62; N, 10.55. Found: C, 45.26; H, 5.71; N, 10.49. IR (KBr, cm⁻¹): 3460(m), 3066(w), 2927(m), 2809(w), 1657(s), 1542(s), 1394(s), 1252(m), 1108(m), 910(w), 864(m), 774(s), 696(s), 530(w), 426(w).

[H₂N(CH₃)₂]₂[Cd(L2)₂].3DMF·H₂O (**2**). **2** was prepared with a procedure similar to that for **1**, except that H₂L1 was replaced by H₂L2. Colorless block crystals of **2** were collected by filtration and washed with DMF. The yield was ca. 19.6 mg (42.5%, based on H₂L2). Anal. Calcd for C₃₉H₅₃CdN₇O₁₂: C, 50.68; H, 5.78; N, 10.61. Found: C, 50.56; H, 5.62; N, 10.48. IR (KBr, cm⁻¹): 3433(w), 3064(w), 2799(w), 2471(w), 1955(w), 1823(w), 1665(s), 1614(s), 1547(s), 1466(m), 1391(s), 1255(w), 1094(m), 1017(m), 854(m), 772(s), 693(m), 524(w), 477(m), 415(w).

[Cd(L3)(H₂O)₂] (**3**). **3** was prepared with a procedure similar to that for **1**, except that H₂L1 was replaced by H₂L3. Colorless block crystals of **3** were collected by filtration and washed with DMF. The yield was ca. 11.7 mg (30.2%, based on H₂L3). Anal. Calcd for C₁₃H₁₁CdNO₆: C, 40.07; H, 2.85; N, 3.60. Found: C, 40.16; H, 2.77; N, 3.53. IR (KBr, cm⁻¹): 3396(w), 3074(w), 2928(w), 1907(w), 1608(s), 1550(s), 1512(m), 1455(w), 1411(s), 1374(s), 1276(m), 1172(m), 1133(m), 1061(m), 909(m), 856(m), 764(s), 710(m), 630(w), 543(w), 435(m).

[Cd(L4)].1.5DMF (**4**). **4** was prepared with a procedure similar to that for **1**, except that H₂L1 was replaced by H₂L4. Colorless block crystals of **4** were collected by filtration and washed with DMF. The yield was ca. 21.9 mg (47.6%, based on H₂L4). Anal. Calcd for C_{17.5}H_{16.5}CdN_{2.5}O_{5.5}: C, 45.47; H, 3.60; N, 7.57. Found: C, 45.42; H, 3.51; N, 7.63. IR (KBr, cm⁻¹): 3385(m), 2928(w), 1660(s), 1589(s), 1488(m), 1403(s), 1367(s), 1268(w), 1195(m), 1100(s), 1061(m), 1030(m), 919(w), 838(m), 775(s), 705(m), 662(m), 556(m), 515(w), 482(m).

X-ray Crystallography. The diffraction experiments for **1–4** were conducted on a Bruker SMART APEX II CCD detector at 296(2) K using Mo K α radiation ($\lambda = 0.71073 \text{ \AA}$) and ω rotation scans at a width of 0.3° . The structures were solved by direct methods and refined by full-matrix least-squares refinements based on F^2 .¹⁵

Table 1. Crystallographic Data and Structural Refinement for 1–4

	1	2	3	4
formula	C ₂₅ H ₃₇ CdN ₅ O ₉	C ₃₉ H ₅₃ CdN ₇ O ₁₂	C ₁₃ H ₁₁ CdNO ₆	C ₁₃ H ₆ CdNO ₄
<i>M_r</i>	664.00	686.99	389.63	352.59
cryst syst	orthorhombic	hexagonal	monoclinic	orthorhombic
space group	<i>Pbcn</i>	<i>P6₃22</i>	<i>P2₁/c</i>	<i>Fdd2</i>
<i>a</i> (Å)	9.4050(10)	18.635(19)	13.678(2)	15.775(6)
<i>b</i> (Å)	20.389(3)	18.635(19)	12.028(2)	16.035(6)
<i>c</i> (Å)	31.799(4)	21.563(4)	7.9500(10)	33.845(14)
α (deg)	90	90	90	90
β (deg)	90	90	98.861(2)	90
γ (deg)	90	120	90	90
<i>V</i> (Å ³)	6097.7(13)	6484.5(16)	1292.3(3)	8561(6)
<i>Z</i>	8	6	4	16
<i>D_{calc}</i> (g cm ⁻³)	1.447	1.056	2.003	1.097
<i>F</i> (000)	2736	2100	768	2752
<i>R_{int}</i>	0.0460	0.0852	0.0216	0.0626
GOF on <i>F</i> ²	1.074	0.987	1.161	1.047
<i>R</i> 1 ^a [<i>I</i> > 2 σ (<i>I</i>)]	0.0600	0.0725	0.0260	0.0786
w <i>R</i> 2 ^b (all data)	0.1772	0.2117	0.1173	0.2129

$${}^a R1 = \sum |F_o| - |F_c| / \sum |F_o|, \quad {}^b wR2 = [\sum w(F_o^2 - F_c^2)^2 / \sum w(F_o^2)^2]^{1/2}.$$

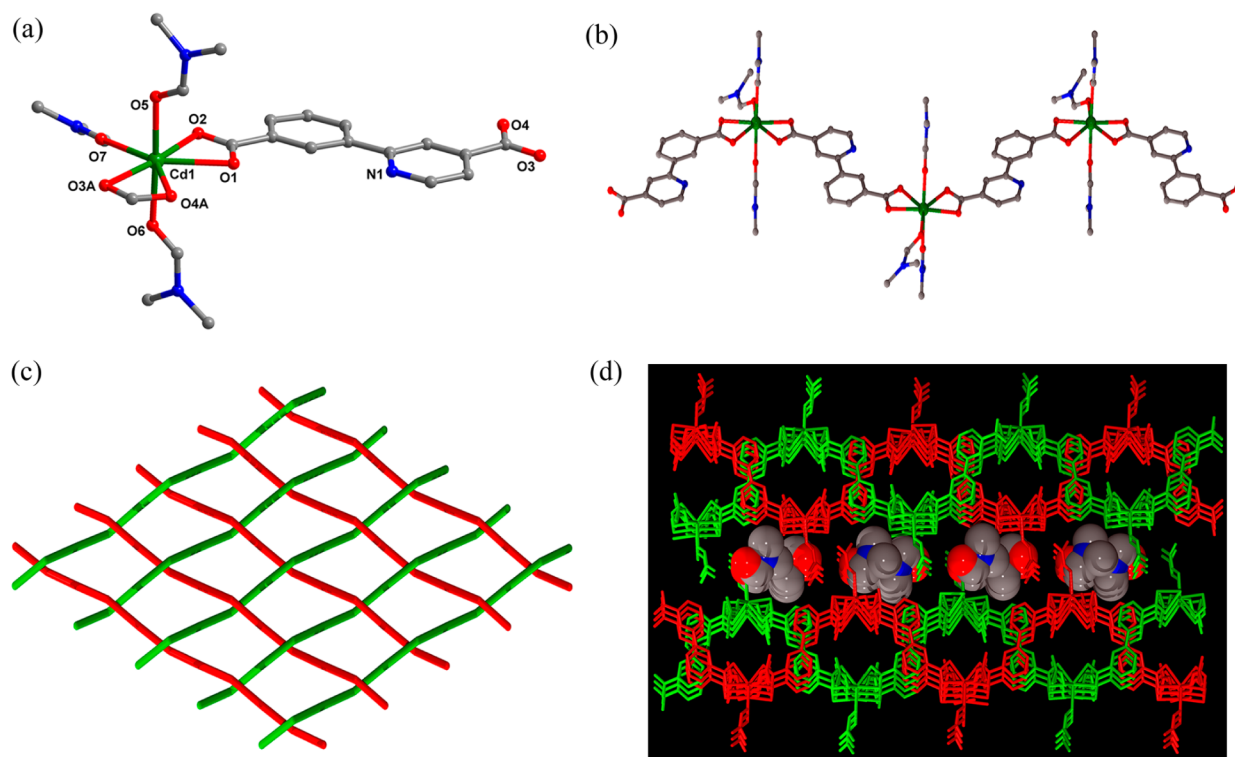


Figure 1. (a) Coordination environment of Cd^{II} ions in 1. (b) 1D undulating chain. (c) View of the fabric structure formed by 1D undulating chains. (d) 3D supramolecular structure of 1. The interlayer spaces are occupied by DMF molecules.

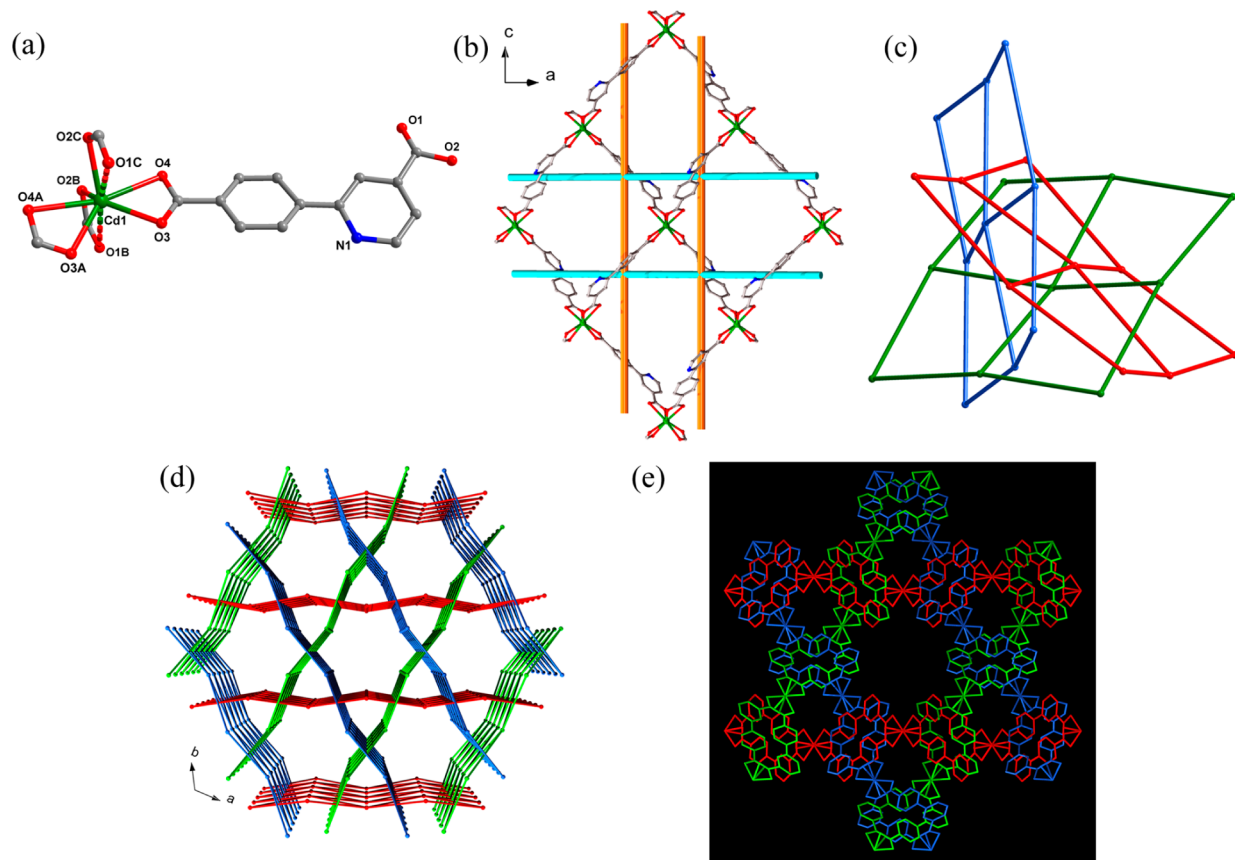


Figure 2. (a) Coordination environment of Cd^{II} ions in 2. (b) Grid layer structure in 2. (c and d) Polycatenation of three sets of grids in different directions with a d-d-d interpenetration mode. (e) 3D framework of 2.

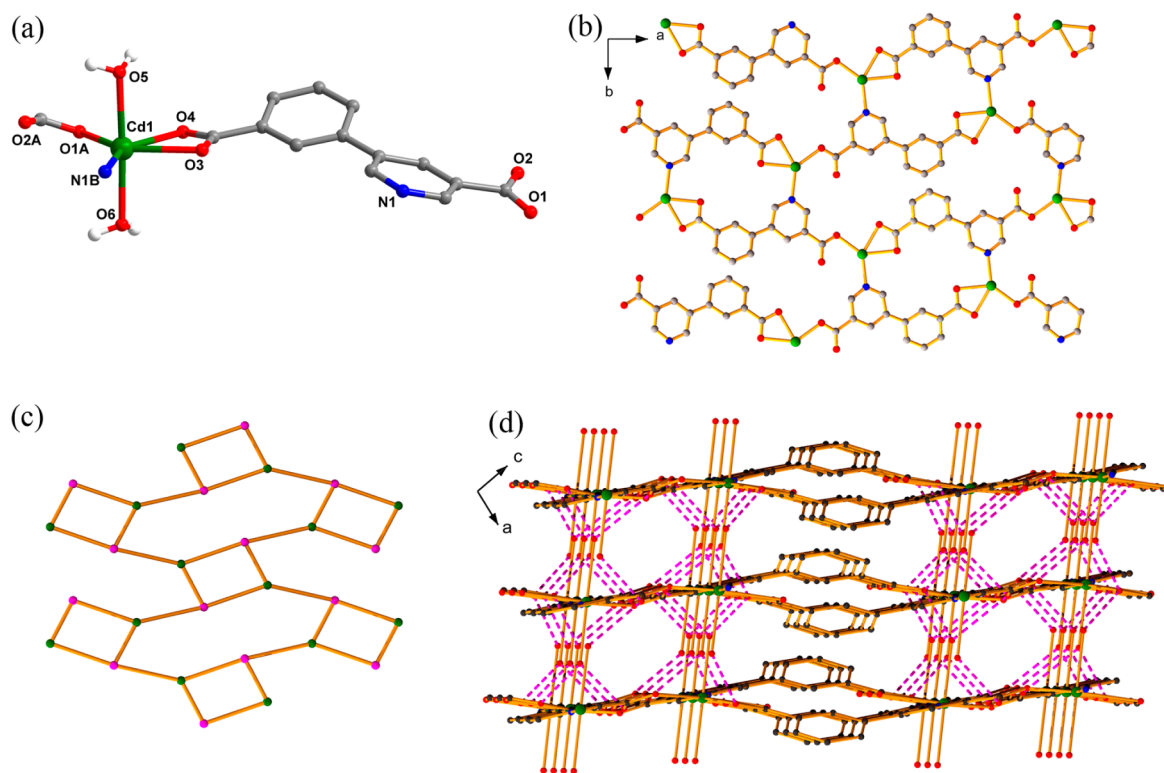


Figure 3. (a) Coordination environment of Cd^{II} ions in **3**. (b and c) 2D layer and its simplified network. (d) 3D supramolecular structure of **3**, in which the purple dotted lines indicate the hydrogen bonds.

Absorption corrections were applied by utilizing the *SADABS* routine. Non-H atoms were refined with anisotropic temperature parameters. H atoms of water and organic molecules were placed in calculated positions and refined with a riding model. Because of the low residual electron density and heavy disorder, it failed to locate the guest molecules in the crystal structures of **2** and **4**. Application of the *SQUEEZE* routine in the *PLATON*¹⁶ software package produced a new intensity data set excluding the intensity contribution from disordered solvent molecules. The final formulas were determined by combining single-crystal structure, elemental microanalysis, IR, and TGA. The crystal data and details of data collection and refinement for **1–4** are summarized in Table 1. CCDC reference numbers for **1–4** are 1482250–1482253 (see the Supporting Information).

Grand Canonical Monte Carlo (GCMC) Simulation Methodology. GCMC simulations were performed for the adsorption of CO₂ in **2** by the *Sorption* module of *Material Studio*.¹⁷ The partial charges for the C and O atoms of CO₂ molecules were 0.576e and −0.288e, respectively.¹⁸ The partial charges for atoms of **2** were derived from the *Qeq* method and *QEq_neutral1.0* parameter (Table S1). The interaction energies between CO₂ and the framework were computed through the Coulomb and Lennard-Jones (LJ) 6–12 potentials. All parameters for the CO₂ molecule and atoms of **2** were modeled with the universal force field embedded in the *MS* modeling package. A cutoff distance of 12.5 Å was used for LJ interactions, and the Coulombic interactions were calculated using the Ewald summation. For each run, 5 × 10⁶ maximum loading steps and 1 × 10⁷ production steps were employed.

RESULTS AND DISCUSSION

Crystal Structure of 1. **1** crystallizes in the orthorhombic space group *Pbcn* and shows an unusual 2D fabric structure. The asymmetric unit of **1** contains one Cd²⁺ ion, one L1^{2−}, and three coordinated DMF molecules. Each Cd²⁺ ion coordinates with seven O atoms from two L1^{2−} and three DMF molecules (Figure 1a). Each L1^{2−} links two Cd²⁺ ions, in which two carboxylate groups adopt the same chelating modes, while the

pyridine N atom is uncoordinated. So, each L1^{2−} acts as a 2-connected node to bridge the adjacent Cd²⁺ ions to give a 1D undulating chain along the [110] or [1 $\bar{1}$ 0] directions, respectively (Figure 1b). Strikingly, the chains in different directions cross one over the other to form a 1O/1U (one over/one under) interwoven layer (Figure 1c), which is stabilized by interchain H₂O molecules that form strong O–H⋯O (O⋯O = 2.946 and 2.999 Å) double hydrogen-bonded interactions with carboxylate O atoms from two adjacent chains (Figure S1). To the best of our knowledge, only five 2D interwoven structures constructed from 1D chains, such as [Cu(2,2′-bpy)(azpy)(H₂O)]·NO₃·H₂O,^{19a} [HgI₂(bpmbpt)],^{19b} [Zn(bac)₂(bpp)]·1.5H₂O,^{19c} [Pb(bpe)(CH₃COO)-(CF₃COO)],^{19d} and [Zn(phen)(sdc)],^{19e} have been reported. **1** presents the second example of a molecular fabric structure based on a single linker.²⁰ Furthermore, in **1**, the neighboring layers are stacked in an ABAB fashion by weak C–H⋯O interactions (C21⋯O2 = 3.429 Å) to produce a 3D supramolecular network (Figure 1d), in which the interlayer spaces are occupied by DMF molecules. The removal of DMF and H₂O molecules provides an accessible void volume of 22.0% (1341.9 Å³ out of the 6097.7 Å³ per unit cell volume), as calculated by *PLATON*.

Crystal Structure of 2. With 2-(4′-carboxylphenyl)-isonicotinic acid instead of 2-(3′-carboxylphenyl)isonicotinic acid, **2** with a 3D polycatenating framework was obtained. **2** crystallizes in the chiral hexagonal space group *P6₁22* and contains half a Cd²⁺ ion and one L2^{2−} in the asymmetric unit. The pyridine N atom of H₂L2 locates at the same position as that of H₂L1, which is also uncoordinated in **2**. Each Cd²⁺ ion coordinates with eight carboxylate O atoms from four L2^{2−} to form a distorted quadrangular prismatic geometry (Figure 2a), with two Cd–O weak bonds (Cd–O = 2.685 Å). Each L2^{2−}

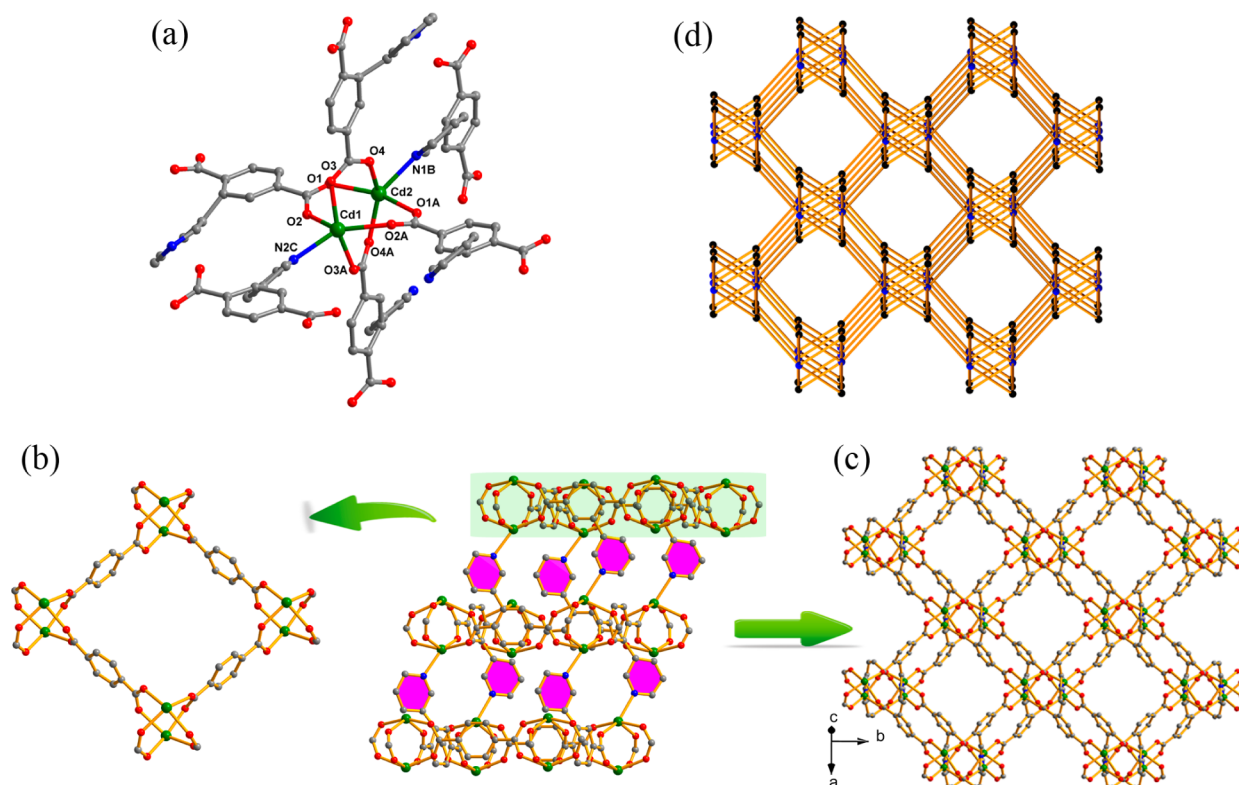


Figure 4. (a) Coordination environment of Cd^{II} ions in **4**. (b) 2D square layer constructed from the $\text{Cd}_2(\text{COO})_4$ units and terephthalate groups. (c) 3D framework of **4** (the purple plane is the pyridine units). (d) Topology network.

bridges two Cd^{2+} ions through the carboxylate groups with a chelating mode, forming a 2D grid layer parallel to the ac crystal plane (Figure 2b). The layer contains two symmetry-related left- and right-handed 2_1 helical chains along the a and c axes, respectively. The most striking feature of **2** is the very uncommon type of $2\text{D} + 2\text{D} + 2\text{D} \rightarrow 3\text{D}$ polycatenation in that three sets of layers exist and stack in three coplanar directions of $[100]$, $[010]$, and $[110]$ (Figure 2c,d), with a relative rotation angle of 60° . Each window in one layer is catenated by the other two different directions of layers with a diagonal–diagonal ($d-d$) type. The interpenetration mode in **2** can be described as $d-d-d$, with a density of catenation of $(2/2/2)$.²¹ To date, very few polycatenating frameworks containing three sets of layers in three coplanar directions are known.²² Meanwhile, most of the reported species display parallel–parallel–parallel ($p-p-p$) interpenetration modes with densities of catenation of $(2/2/2)$ ^{22a-c} and $(2/4/4)$,^{22d} and only one case shows $d-d-d$ interpenetration modes but with a different density of catenation of $(1/1/1)$ ^{22e} compared to **2**. Thereby **2** represents the first example of a $2\text{D} + 2\text{D} + 2\text{D} \rightarrow 3\text{D}$ polycatenating framework by interlayer inclined interpenetration with $d-d-d$ mode and a density of catenation of $(2/2/2)$. Such a unique interpenetration in **2** produces trigonal ($3.6 \times 3.6 \text{ \AA}^2$, excluding van der Waals radii of the atoms) and hexagonal ($5.2 \times 5.2 \text{ \AA}^2$) channels along the c axis. Meanwhile, relatively narrow channels also exist along the a and b axes (Figure S2). The three channels are intersected to form a 3D continuous porous space with 56.0% free voids, which is filled by guest molecules and $\text{H}_2\text{N}(\text{CH}_3)_2$ cations derived from the decomposition of DMF molecules. The uncoordinated pyridine groups point toward the inner surfaces of the pores.

Crystal Structure of 3. Compared to $\text{H}_2\text{L1}$, the position of the pyridine N atom of $\text{H}_2\text{L3}$ is changed. Under synthetic

conditions similar to those of **1**, **3** was obtained, which crystallizes in the monoclinic space group $P2_1/c$ and shows a 2D layer. The asymmetric unit is composed of one Cd^{2+} ion, one L3^{2-} , and two coordinated H_2O molecules (Figure 3a). Different from **1** and **2**, the pyridine N atom of L3^{2-} in **3** is coordinated. The Cd^{2+} ion shows a distorted octahedral geometry defined by three carboxylate O atoms and one N atom of three L3^{2-} and two water O atoms. Because of the axial positions of Cd^{2+} , the coordination sphere is occupied by H_2O molecules, and each Cd^{2+} ion links three 3-connected L3^{2-} to form a layer parallel to the ab crystal plane (Figure 3b). Strong intralayer $\pi \cdots \pi$ interactions exist (the vertical distance between phenyls is 3.299 \AA ; Figure S3). The adjacent 2D layers stack in an AAA fashion and form hydrogen bonds between the coordinated H_2O molecules (O5 and O6) and two carboxylate O2 and O4 atoms ($\text{O2} \cdots \text{O5} = 3.006 \text{ \AA}$, $\text{O4} \cdots \text{O5} = 2.828 \text{ \AA}$, $\text{O2} \cdots \text{O6} = 2.761 \text{ \AA}$, and $\text{O4} \cdots \text{O6} = 2.751 \text{ \AA}$), giving rise to a 3D supramolecular framework (Figure 3d).

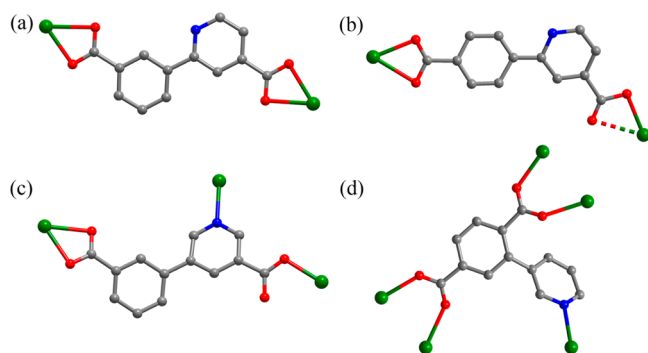
Crystal Structure of $[\text{Cd}(\text{L4})] \cdot 2\text{DMF}$ (4). Compared to $\text{H}_2\text{L3}$, the position of one carboxyl group is changed to form $\text{H}_2\text{L4}$. The reaction of $\text{H}_2\text{L4}$ with a Cd^{2+} ion yields a 3D framework of **4** with the orthorhombic space group $Fdd2$ consists of two Cd^{2+} ions and two L4^{2-} in the asymmetric unit. As shown in Figure 4a, four carboxylate groups of four different L4^{2-} connect two Cd^{2+} ions to generate a paddle-wheel unit with a $\text{Cd} \cdots \text{Cd}$ separation of 3.442 \AA , in which the axial positions of Cd^{2+} coordination spheres are occupied by two pyridine N atoms of two different L4^{2-} . It should be noted that the $\text{M}_2(\text{COO})_4$ paddle-wheel units are widely found in Cu^{2+} , Co^{2+} , Zn^{2+} , and Mn^{2+} complexes; however, the Cd^{2+} case remains rarely known,²³ especially in 3D CPs.^{23f-h}

For a clearer understanding on the structure of **4**, the bridging fashion of L4^{2-} can be segmented as the combination

of terephthalate and pyridine units. The $\text{Cd}_2(\text{COO})_4$ units are connected by terephthalates to furnish a 2D square layer parallel to the *ab* crystal plane (Figure 4b). The layers are pillared by pyridine units of L^{2-} to form a 3D porous framework with solvent-accessible voids of 41.7% (Figure 4c). The framework contains rectangular channels along the [101] direction with opening sizes of about $5.6 \times 5.6 \text{ \AA}^2$. Considering the $\text{Cd}_2(\text{COO})_4$ unit and L^{2-} as 6- and 3-connected nodes, respectively, 4 forms a (3,6)-connected binodal ant net with the topology symbol of $(4^2 \cdot 6)_2(4^4 \cdot 6^2 \cdot 8^8 \cdot 10)$ (Figure 4d).

Positional Effects of Coordination Sites on the Structures. In 1 and 2, both L^{1-} and L^{2-} as 2-connected nodes display similar coordination modes, in which the carboxyl groups exhibit a $\mu_1:\eta_1:\eta_1$ coordination mode (Scheme 2a,b), while the pyridine N atom is uncoordinated because of

Scheme 2. Different Bridging Fashions of H_2L in 1 (a), 2 (b), 3 (c), and 4 (d)



steric hindrance from the H atom of the phenyl ring. The two carboxylates of L^{1-} in 1 form an arrangement of about 180° , and it is about 120° for L^{2-} in 2. This different connection direction leads to two distinct structures, a 1D chain for 1 and a 2D layer for 2, which further form an uncommon 2D fabric layer and $2\text{D} + 2\text{D} + 2\text{D} \rightarrow 3\text{D}$ polycatenation, respectively. $\text{H}_2\text{L}1$ and $\text{H}_2\text{L}3$ possess very similar geometry except that the pyridine N atom from the ortho position of benzoic acid in $\text{H}_2\text{L}1$ is moved to the meta position of benzoic acid in $\text{H}_2\text{L}3$, which makes the pyridine N atom of L^{3-} coordinate and forms a 2D layer structure of 3 but not a 1D chain as shown in 1. Meanwhile, the two carboxylates of L^{3-} in 3 exhibit $\mu_1:\eta_1:\eta_1$ and $\mu_1:\eta_0:\eta_1$ coordination modes, respectively (Scheme 2c). In contrast, the two carboxylates of L^{4-} in 4 locate at one phenyl unit and display a $\mu_2:\eta_1:\eta_1$ coordination fashion (Scheme 2d).

In addition, the four isomeric ligands show different electron-conjugated systems with an order of $\text{H}_2\text{L}2 > \text{H}_2\text{L}1 > \text{H}_2\text{L}3 > \text{H}_2\text{L}4$ (Figure S4). The electron-conjugated effect of ligand molecules is important for their structural configurations in frameworks, which leads to the formation of not only different torsion angles of the ligands but also distinct structure symmetries of the final frameworks. Obviously, because of the small torsion angles for the two aryls of 17.06° in L^{1-} and 14.16° in L^{2-} , the pyridine N atoms are uncoordinated; in contrast, the corresponding angles are bigger in L^{3-} (39.21°) and L^{4-} (61.51°), leading to coordination of the pyridine groups. Such a high torsion angle in L^{4-} is conducive to expanding the connection direction and to forming the 3D porous framework of 4. The above results reveal the significant effect of the positions of the carboxyl and pyridyl groups on the final structures.

PXRD and TGA. The experimental PXRD patterns of 1–4 are in agreement with the simulated ones from the single-crystal structures (Figure S5), indicating the phase purity. TGA was performed under a N_2 atmosphere on the polycrystalline samples of 1–4 (Figure S6). For 1, the TGA curve exhibits the first weight loss of about 46.7% within the temperature range $70\text{--}325^\circ\text{C}$, which is ascribed to the release of all DMF and H_2O molecules (calcd, 46.6%), and then the residual framework starts to decompose. For 2, the preliminary weight loss in the range $30\text{--}145^\circ\text{C}$ is attributed to the loss of guest DMF and H_2O molecules (found, 25.4%; calcd, 25.7%), and then a thermally stable flat is followed before structural decomposition at 350°C . For 3, the weight loss of 9.5% in the range $30\text{--}188^\circ\text{C}$ corresponds to the removal of all H_2O ligands (calcd, 9.2%). Above 360°C , a further heating induces decomposition of 3. For 4, the weight loss of about 23.6% within the temperature range $30\text{--}205^\circ\text{C}$ is due to the release of DMF molecules (calcd, 23.7%), and then there is no further weight loss before structural decomposition at 305°C . The solvent molecules in 2 and 4 can be completely removed by soaking the samples in CH_3OH for 72 h and subsequently heating at 80°C under a vacuum for 6 h. Then guest-free phases, 2a and 4a, were verified by TGA and IR (Figures S6 and S7). PXRD patterns demonstrate the framework integrity of 2a and 4a (Figure S5), and the weakening and slight shifting of some peaks for 2a should be attributed to the slight framework distortion due to solvent release.

Sorption Properties. Gas-adsorption measurements (N_2 , H_2 , CO_2 , and CH_4) were performed to evaluate the porosity of 2a and 4a. As shown in Figure 5a, the N_2 and H_2 sorption

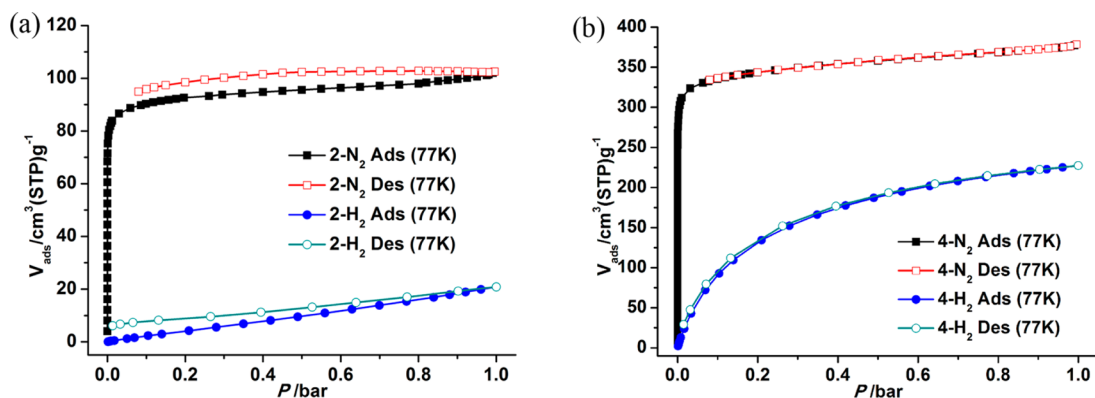


Figure 5. N_2 and H_2 sorption isotherms of 2a (a) and 4a (b) measured at 77 K.

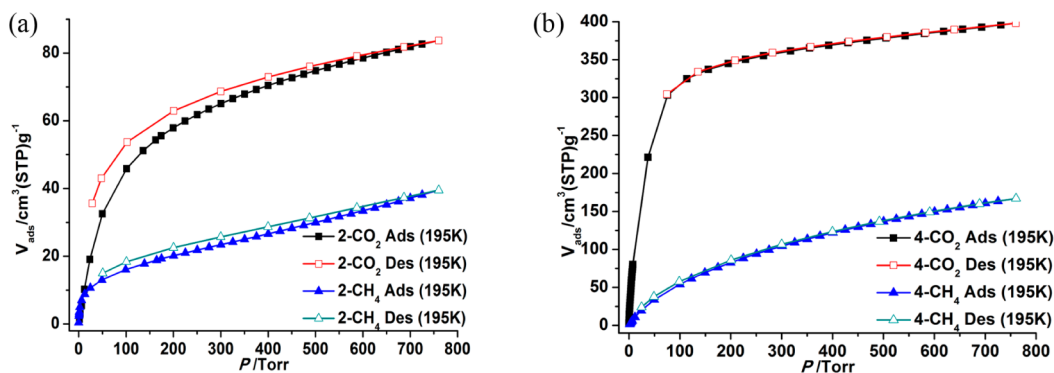


Figure 6. CO₂ and CH₄ sorption isotherms of **2a** (a) and **4a** (b) measured at 195 K.

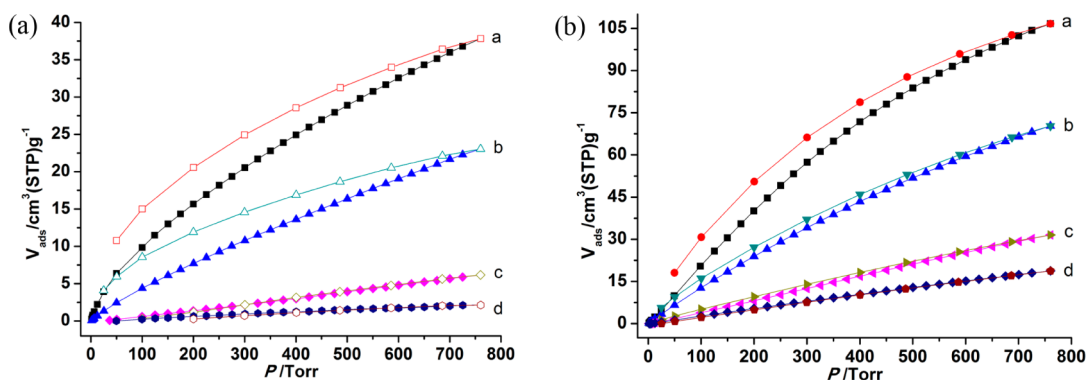


Figure 7. Sorption isotherms of **2a** (a) and **4a** (b): CO₂ at 273 K (a) and 298 K (b); CH₄ at 273 K (c) and 298 K (d).

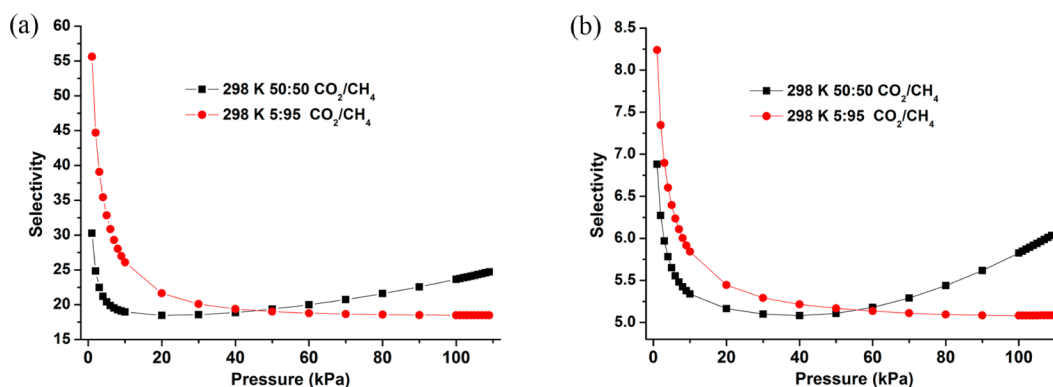


Figure 8. IAST adsorption selectivity of **2a** (a) and **4a** (b) for CO₂ over CH₄ at different compositions.

isotherms of **2a** and **4a** at 77 K show the characteristics of microporous materials, but **2a** displays obvious hysteresis curves. The desorption hysteresis is mainly related to the narrow channel system in **2a**, which blocks the departure of adsorbed gas molecules.²⁴ The Brunauer–Emmett–Teller and Langmuir surface areas are 369 and 402 m² g⁻¹ for **2a** and 1376 and 1509 m² g⁻¹ for **4a**, respectively. The total microporous volumes are 0.16 and 0.59 m³ g⁻¹ for **2a** and **4a**, respectively. The measured pore-size-distribution curves based on the density functional theory model show the main pore sizes of 3.9–5.4 and 5.0–6.8 Å for **2a** and **4a**, respectively (Figure S8). In contrast to the low H₂ uptake of **2a** at 77 K, **4a** exhibits an excellent H₂ storage capacity of 227.2 m³ g⁻¹ (2.03 wt %) at 1 atm (Figure S5b), which is comparable to the highest capacity values in PCN-6 (1.9 wt %),^{25a} DUT-6 (2.02 wt %),^{25b} DMOF-1–NH₂ (2.08 wt %),^{25c} and SNU-4 (2.07%).^{25d}

The CO₂ and CH₄ sorption isotherms of **2a** and **4a** at 195 K were also measured (Figure 6). For **2a**, the CO₂ and CH₄ uptakes at 1 atm are 83.6 cm³ g⁻¹ (16.4 wt %) and 39.4 cm³ g⁻¹ (2.8 wt %), respectively. For **4a**, at 1 atm, the CO₂ uptake reaches 313.0 cm³ g⁻¹ (61.5 wt %), corresponding to 5.0 CO₂ molecules per formula unit, and the CH₄ uptake is 127.3 cm³ g⁻¹ (9.1 wt %). The CH₄ adsorption amounts of **2a** and **4a** are much lower than the values of the CO₂ uptakes. The preferred CO₂ adsorption properties of **2a** and **4a** encourage us to examine their potential application for CO₂–CH₄ separation at ambient temperature. As shown in Figure 7, the CO₂ uptakes at 1 atm are 37.8 cm³ g⁻¹ (7.4 wt %) and 106.6 cm³ g⁻¹ (20.9 wt %) at 273 K and 23.0 cm³ g⁻¹ (4.5 wt %) and 70.3 cm³ g⁻¹ (13.8 wt %) at 298 K for **2a** and **4a**, respectively. The CO₂ uptake of **4a** at 298 K and 1 atm is slightly higher than that of MAF-23 (11.0 wt %), which possesses multiple strong adsorption sites,²⁶ and comparable to some recently reported

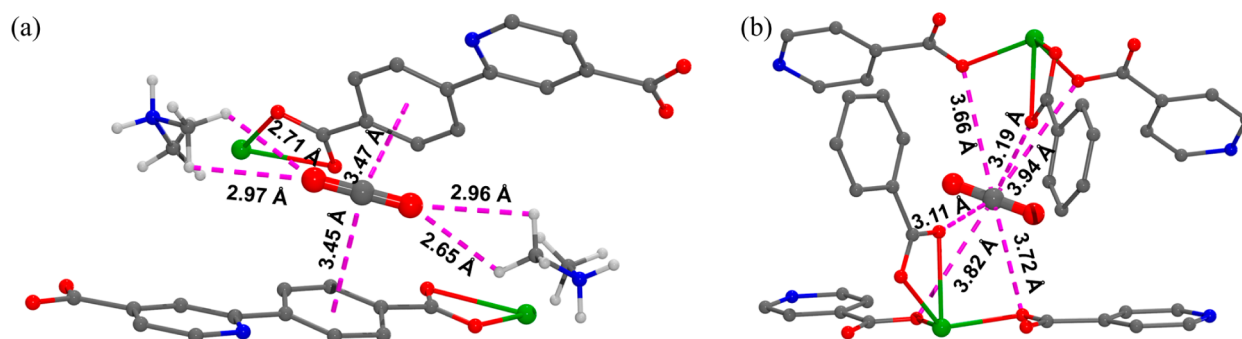


Figure 9. Simulated favorable CO₂ sorption sites in 2a: (a) site I; (b) site II.

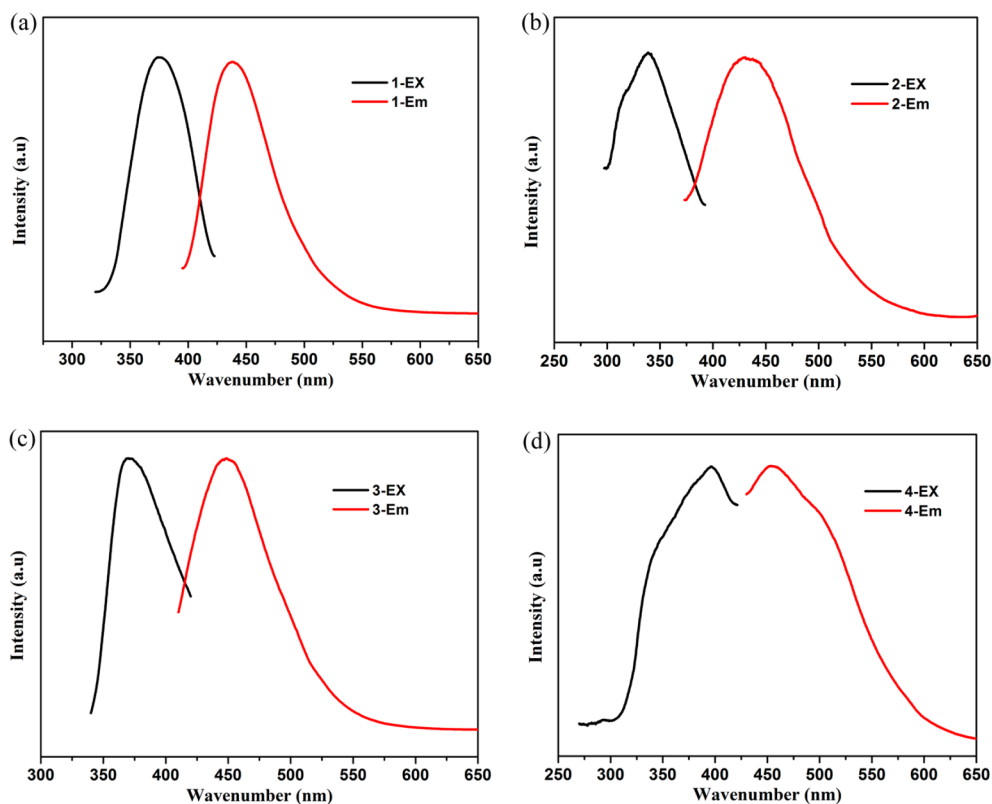


Figure 10. Solid-state excitation and emission spectra of 1–4 at room temperature.

metal–organic frameworks (MOFs) based on excellently designed structure, such as rht-MOF-pyr (13.0 wt %),^{27a} Cd–L (15.5 wt %),^{27b} and Cu₄[(C₅₇H₃₂N₁₂)(COO)₈] (14.5 wt %).^{27c} The larger desorption hysteresis of CO₂ in 2a suggests stronger interactions of the framework of 2a with CO₂ than that of 4a. At 1 atm, the CH₄ uptakes of 2a and 4a are 6.2 and 31.5 cm³ g^{−1} at 273 K and 2.1 and 18.8 cm³ g^{−1} at 298 K, respectively. The CO₂/CH₄ selectivities of 2a and 4a under mixture gas conditions at 298 K can be estimated by the ideal adsorbed solution theory²⁸ (IAST; Figure S9). For CO₂/CH₄ mixtures with general feed compositions of landfill gas (50:50 CO₂/CH₄) and natural gas (5:95 CO₂/CH₄), the CO₂/CH₄ selectivities calculated at 1 atm are 24.7 and 18.5 for 2a and 6.0 and 5.1 for 4a, respectively (Figure 8). These values in 2a are higher than many famous MOFs such as HKUST-1 (2.28), MIL-53(Al) (2.30), and ZIF-8 (1.32)²⁹ and approximate with those in MPM-1-TIFSIX (20.3)^{30a} and [Cu₃(TDPAH)(H₂O)₃] (18.0).^{30b} Notably, by a comparison of the CO₂/CH₄ selectivities in 2a and 4a with those known MOFs that

possessed good CO₂/CH₄ selectivity (Table S2), it is clearly indicated that the CO₂/CH₄ selectivity in 2a is significantly high, ranking in the top region.

The adsorption selectivities of 2a and 4a for CO₂ are closely related to the smaller kinetic diameter of CO₂ compared to that of CH₄ (CO₂, 3.3 Å; CH₄, 3.8 Å), as well as the larger quadrupole moment and higher polarizability value of CO₂ relative to CH₄. The considerable difference of the CO₂/CH₄ selectivity values for 2a and 4a relies on the different structure features. The more remarkable CO₂ sorption selectivity of 2a should be attributed to the anionic framework that generates a significantly electric field, while the free pyridine N atoms of L^{2−} and H₂N(CH₃)₂ cations can easily approach CO₂ molecules.³¹ To estimate the strength of framework–CO₂ interactions, the isosteric heat of adsorption (*Q*_{st}) was calculated via the virial method by fitting the adsorption curves collected at 273 and 298 K (Figures S10 and S11). The *Q*_{st} value of 2a for CO₂ is 37.2 kJ mol^{−1} at initial coverage, indicating strong CO₂–framework interactions. In contrast, 4a

reveals low Q_{st} values (5.8–18.1 kJ mol⁻¹) of CO₂ because of the lack of classical interacting sites such as open metal sites and/or free amine groups within the framework.³² Only the aromatic sites in **4a** afford an affinity toward CO₂ molecules, leading to a relatively low CO₂/CH₄ selectivity compared to **2a**.

GCMC Simulations. The interaction mechanism between the framework of **2a** and CO₂ can be identified by GCMC simulations. The results indicate two main adsorption sites existing in **2a**. The first site is located at the center of two H₂N(CH₃)₂ cations (Figure 9a), in which the two electro-negative O atoms of CO₂ form two pairs of C–H···O_{CO₂} hydrogen bonds with the four methyl H atoms of two H₂N(CH₃)₂ cations, and the H···O_{CO₂} distances of 2.65–2.97 Å are comparable to the sum of the van der Waals radii of H (1.20 Å) and O (1.52 Å) atoms, implying significant interactions. Meanwhile, in this site, the CO₂ molecule is parallel with the phenyl rings of two L2²⁻ from two layers; consequently, the electropositive C atom of CO₂ also forms strong C_{CO₂}··· π interactions with the two phenyl rings, and the C_{CO₂}··· $\pi_{centroid}$ distances of 3.45 and 3.47 Å are shorter than those reported in other MOFs.³³ The increase of CO₂ loading makes the other adsorption site available, which is near the middle of two coordination motifs from two layers (Figure 9b). As a result, the C atoms of the CO₂ molecules form C_{CO₂}···O contacts with the coordinated electronegative carboxylate O atoms. The C_{CO₂}···O distance (3.11–3.94 Å) is close to the sum of the van der Waals radii of C (1.70 Å) and O atoms, suggesting moderate interactions. These multiple framework–CO₂ interactions lead to the relatively high adsorption heat of **2** for CO₂ and significant CO₂/CH₄ selectivity.

Photoluminescence Properties. The solid-state photoluminescence of **1–4** (Figure 10) and free ligands H₂L1–H₂L4 (Figure S12) was investigated at room temperature. The emission spectra in the blue region have broad peaks with maxima at 439 nm (λ_{ex} = 376 nm) for **1**, 433 nm (λ_{ex} = 338 nm) for **2**, 448 nm (λ_{ex} = 370 nm) for **3**, and 455 nm (λ_{ex} = 396 nm) for **4**. These bands can be assigned to $\pi^* \rightarrow \pi$ or $\pi^* \rightarrow n$ intraligand charge transfer because similar emissions are observed at 432 nm for H₂L1, 405 nm for H₂L2, 409 nm for H₂L3, and 400 and 470 nm for H₂L4.

CONCLUSION

In summary, we have constructed four CPs based on four isomeric pyridyldicarboxylate acid ligands with different coordination sites. **1–4** display charming structural features, including an uncommon 2D fabric structure of **1**, a rare 2D + 2D + 2D → 3D polycatenation of **2** based on the interpenetration of three sets of layers, featuring an unprecedented d–d–d interpenetration mode with a density of catenation of (2/2/2), a 3D supramolecular framework of **3**, and a 3D porous framework of **4** based on the scarce Cd₂(COO)₄ paddle-wheel units. The results demonstrate the significant effect of the positions of the carboxyl and pyridyl groups on the final structures. **1–4** exhibit solid-state blue luminescence with different emission energies; meanwhile, **2a** and **4a** also display gas-adsorption performances. **2a** because of the existence of multiple adsorption sites displays better adsorption selectivity for CO₂ over CH₄. The significant CO₂ adsorption selectivity and capacity enable **2a** and **4a** to be the promising candidates for capturing CO₂ from natural gas. This work would provide further insight into the design of new

functional crystalline materials from the positional isomeric ligands for regulating structural assembly.

ASSOCIATED CONTENT

Supporting Information

The Supporting Information is available free of charge on the ACS Publications website at DOI: 10.1021/acs.inorgchem.6b01416.

X-ray crystallographic data of **1** in CIF format (CIF)
 X-ray crystallographic data of **2** in CIF format (CIF)
 X-ray crystallographic data of **3** in CIF format (CIF)
 X-ray crystallographic data of **4** in CIF format (CIF)
 Additional structural figures, PXRD patterns, TGA plots, and FTIR spectra of **1–4**, detailed calculations on sorption, and solid emission spectra of free ligands (PDF)

AUTHOR INFORMATION

Corresponding Author

*E-mail: lhou2009@nwu.edu.cn (L.H.).

Notes

The authors declare no competing financial interest.

ACKNOWLEDGMENTS

This work is supported by the National Science Foundation of China (Grants 21471124 and 21531007), the National Science Foundation of Shannxi Province (Grants 2013KJXX-26, 2014JQ2049, and 15JS113), a Ph.D. Start-up Fund of Northwest A&F University (Grant 2452015359), and an Australian Research Council Future Fellowship (Grant FT12010072).

REFERENCES

- (1) (a) Allendorf, M. D.; Bauer, C. A.; Bhakta, R. K.; Houk, R. J. T. *Chem. Soc. Rev.* **2009**, *38*, 1330–1352. (b) Cui, Y.; Yue, Y.; Qian, G.; Chen, B. *Chem. Rev.* **2012**, *112*, 1126–1162. (c) Hu, Z.; Lustig, W. P.; Zhang, J.; Zheng, C.; Wang, H.; Teat, S. J.; Gong, Q.; Rudd, N. D.; Li, J. *J. Am. Chem. Soc.* **2015**, *137*, 16209–16215.
- (2) (a) Deng, H.; Grunder, S.; Cordova, K. E.; Valente, C.; Furukawa, H.; Hmadeh, M.; Gándara, F.; Whalley, A. C.; Liu, Z.; Asahina, S.; Kazumori, H.; O’Keeffe, M.; Terasaki, O.; Stoddart, J. F.; Yaghi, O. M. *Science* **2012**, *336*, 1018–1023. (b) Li, J.-R.; Sculley, J.; Zhou, H.-C. *Chem. Rev.* **2012**, *112*, 869–932.
- (3) Chughtai, A. H.; Ahmad, N.; Younus, H. A.; Laypkov, A.; Verpoort, F. *Chem. Soc. Rev.* **2015**, *44*, 6804–6849.
- (4) (a) Fu, H.-R.; Xu, Z.-X.; Zhang, J. *Chem. Mater.* **2015**, *27*, 205–210. (b) Yang, Y.; Jiang, F.; Chen, L.; Pang, J.; Wu, M.; Wan, X.; Pan, J.; Qian, J.; Hong, M. *J. Mater. Chem. A* **2015**, *3*, 13526–13532.
- (5) (a) Xiao, J.; Liu, B.-Y.; Wei, G.; Huang, X.-C. *Inorg. Chem.* **2011**, *50*, 11032–11038. (b) Li, C.-P.; Du, M. *Chem. Commun.* **2011**, *47*, 5958–5972. (c) Rosa, I. M. L.; Costa, M. C. S.; Vitto, B. S.; Amorim, L.; Correa, C. C.; Pinheiro, C. B.; Doriguetto, A. C. *Cryst. Growth Des.* **2016**, *16*, 1606–1616.
- (6) (a) Zhang, W.-X.; Liao, P.-Q.; Lin, R.-B.; Wei, Y.-S.; Zeng, M.-H.; Chen, X.-M. *Coord. Chem. Rev.* **2015**, *293–294*, 263–278. (b) Xu, H.-Q.; Wang, K.; Ding, M.; Feng, D.; Jiang, H.-L.; Zhou, H.-C. *J. Am. Chem. Soc.* **2016**, *138*, 5316–5320. (c) Zhang, Z.; Zaworotko, M. J. *Chem. Soc. Rev.* **2014**, *43*, 5444–5455.
- (7) (a) Lu, W.; Wei, Z.; Gu, Z.-Y.; Liu, T.-F.; Park, J.; Park, J.; Tian, J.; Zhang, M.; Zhang, Q.; Gentle, T., III; Bosch, M.; Zhou, H.-C. *Chem. Soc. Rev.* **2014**, *43*, 5561–5593. (b) Du, M.; Li, C.-P.; Chen, M.; Ge, Z.-W.; Wang, X.; Wang, L.; Liu, C.-S. *J. Am. Chem. Soc.* **2014**, *136*, 10906–10909. (c) Xuan, Z.-H.; Zhang, D.-S.; Chang, Z.; Hu, T.-L.; Bu, X.-H. *Inorg. Chem.* **2014**, *53*, 8985–8990. (d) Xu, Z.-X.; Tan, Y.-X.; Fu, H.-R.; Liu, J.; Zhang, J. *Inorg. Chem.* **2014**, *53*, 12199–12204.

- (e) Zhao, D.; Timmons, D. J.; Yuan, D.; Zhou, H.-C. *Acc. Chem. Res.* **2011**, *44*, 123–133.
- (8) (a) Yin, Z.; Zhou, Y.-L.; Zeng, M.-H.; Kurmoo, M. *Dalton Trans.* **2015**, *44*, 5258–5275. (b) Qian, J.; Jiang, F.; Su, K.; Pan, J.; Liang, L.; Mao, F.; Hong, M. *Cryst. Growth Des.* **2015**, *15*, 1440–1445. (c) Aulakh, D.; Varghese, J. R.; Wriedt, M. *Inorg. Chem.* **2015**, *54*, 1756–1764. (d) Liu, L.-L.; Yu, C.-X.; Li, Y.-R.; Han, J.-J.; Ma, F.-J.; Ma, L.-F. *CrystEngComm* **2015**, *17*, 653–664. (e) Schoedel, A.; Boyette, W.; Wojtas, L.; Eddaoudi, M.; Zaworotko, M. J. *J. Am. Chem. Soc.* **2013**, *135*, 14016–14019.
- (9) (a) Cheng, P.-C.; Wu, M.-H.; Xie, M.-Y.; Huang, W.-J.; He, H.-Y.; Wu, T.-T.; Lo, Y.-C.; Proserpio, D. M.; Chen, J.-D. *CrystEngComm* **2013**, *15*, 10346–10357. (b) Hsu, Y.-F.; Hu, H.-L.; Wu, C.-J.; Yeh, C.-W.; Proserpio, D. M.; Chen, J.-D. *CrystEngComm* **2009**, *11*, 168–176. (c) Chi, Y.-N.; Huang, K.-L.; Cui, F.-Y.; Xu, Y.-Q.; Hu, C.-W. *Inorg. Chem.* **2006**, *45*, 10605–10612. (d) Chi, Y.-N.; Cui, F.-Y.; Xu, Y.-Q.; Hu, C.-W. *Eur. J. Inorg. Chem.* **2007**, *2007*, 4375–4384. (e) Zhu, P.-P.; Sun, L.-J.; Sheng, N.; Sha, J.-Q.; Liu, G.-D.; Yu, L.; Qiu, H.-B.; Li, S.-X. *Cryst. Growth Des.* **2016**, *16*, 3215–3223.
- (10) (a) Cheng, P.-C.; Kuo, P.-T.; Liao, Y.-H.; Xie, M.-Y.; Hsu, W.; Chen, J.-D. *Cryst. Growth Des.* **2013**, *13*, 623–632. (b) Liu, T.; Wang, S.; Lu, J.; Dou, J.; Niu, M.; Li, D.; Bai, J. *CrystEngComm* **2013**, *15*, 5476–5489. (c) Guo, F.; Wang, F.; Yang, H.; Zhang, X.; Zhang, J. *Inorg. Chem.* **2012**, *51*, 9677–9682. (d) Ma, L.-F.; Li, X.-Q.; Meng, Q.-L.; Wang, L.-Y.; Du, M.; Hou, H.-W. *Cryst. Growth Des.* **2011**, *11*, 175–184.
- (11) (a) Xiang, S.; Huang, J.; Li, L.; Zhang, J.; Jiang, L.; Kuang, X.; Su, C.-Y. *Inorg. Chem.* **2011**, *50*, 1743–1748. (b) Zhang, P.; Li, B.; Zhao, Y.; Meng, X.; Zhang, T. *Chem. Commun.* **2011**, *47*, 7722–7724. (c) Cui, P.-P.; Zhang, X.-D.; Zhao, Y.; Chen, K.; Wang, P.; Sun, W.-Y. *Microporous Mesoporous Mater.* **2015**, *208*, 188–195. (d) Luo, X.; Sun, L.; Zhao, J.; Li, D.-S.; Wang, D.; Li, G.; Huo, Q.; Liu, Y. *Cryst. Growth Des.* **2015**, *15*, 4901–4907.
- (12) (a) Liu, Y.; Li, J.-R.; Verdegaal, W. M.; Liu, T.-F.; Zhou, H.-C. *Chem. - Eur. J.* **2013**, *19*, 5637–5643. (b) Du, L.; Lu, Z.; Zheng, K.; Wang, J.; Zheng, X.; Pan, Y.; You, X.; Bai, J. *J. Am. Chem. Soc.* **2013**, *135*, 562–565.
- (13) (a) Schnobrich, J. K.; Lebel, O.; Cychosz, K. A.; Dailly, A.; Wong-Foy, A. G.; Matzger, A. J. *J. Am. Chem. Soc.* **2010**, *132*, 13941–13948. (b) Xie, Y.; Yang, H.; Wang, Z. U.; Liu, Y.; Zhou, H.-C.; Li, J.-R. *Chem. Commun.* **2014**, *50*, 563–565.
- (14) (a) Liu, B.; Li, Y.; Hou, L.; Yang, G.; Wang, Y.-Y.; Shi, Q.-Z. *J. Mater. Chem. A* **2013**, *1*, 6535–6538. (b) Liu, B.; Wei, L.; Li, N.; Wu, W.-P.; Miao, H.; Wang, Y.-Y.; Shi, Q.-Z. *Cryst. Growth Des.* **2014**, *14*, 1110–1127. (c) Liu, B.; Wu, W.-P.; Hou, L.; Li, Z.-S.; Wang, Y.-Y. *Inorg. Chem.* **2015**, *54*, 8937–8942.
- (15) Sheldrick, G. M. *SHELXL-97, program for the refinement of the crystal structures*; University of Göttingen: Göttingen, Germany, 1997.
- (16) Spek, A. L. *J. Appl. Crystallogr.* **2003**, *36*, 7–13.
- (17) *Accelrys, Materials Studio Getting Started*, release 5.0; Accelrys Software, Inc.: San Diego, CA, 2009.
- (18) Hirotani, A.; Mizukami, K.; Miura, R.; Takaba, H.; Miya, T.; Fahmi, A.; Stirling, A.; Kubo, M.; Miyamoto, A. *Appl. Surf. Sci.* **1997**, *120*, 81–84.
- (19) (a) Carlucci, L.; Ciani, G.; Gramaccioli, A.; Proserpio, D. M.; Rizzato, S. *CrystEngComm* **2000**, *2*, 154–163. (b) Li, Y.-H.; Su, C.-Y.; Goforth, A. M.; Shimizu, K. D.; Gray, K. D.; Smith, M. D.; zur Loye, H.-C. *Chem. Commun.* **2003**, 1630–1631. (c) Han, L.; Zhou, Y. *Inorg. Chem. Commun.* **2008**, *11*, 385–387. (d) Peedikakkal, A. M. P.; Vittal, J. J. *Cryst. Growth Des.* **2008**, *8*, 375–377. (e) Cheng, A.-L.; Liu, N.; Yue, Y.-F.; Jiang, Y.-W.; Gao, E.-Q.; Yan, C.-H.; He, M.-Y. *Chem. Commun.* **2007**, 407–409.
- (20) Leong, W. L.; Vittal, J. J. *Chem. Rev.* **2011**, *111*, 688–764.
- (21) Carlucci, L.; Ciani, G.; Proserpio, D. M. *Coord. Chem. Rev.* **2003**, *246*, 247–289.
- (22) (a) Chen, B.; Jiang, F.; Han, L.; Wu, B.; Yuan, D.; Wu, M.; Hong, M. *Inorg. Chem. Commun.* **2006**, *9*, 371–374. (b) Zhuang, W. J.; Zheng, X. J.; Li, L. C.; Liao, D. Z.; Ma, H.; Jin, L. P. *CrystEngComm* **2007**, *9*, 653–667. (c) Wang, S.; Wang, D.; Dou, J.; Li, A. *Acta Crystallogr., Sect. C: Cryst. Struct. Commun.* **2010**, *66*, m141–m144. (d) Carlucci, L.; Ciani, G.; Proserpio, D. M.; Rizzato, S. *CrystEngComm* **2003**, *5*, 190–199. (e) Du, L.-Y.; Shi, W.-J.; Hou, L.; Wang, Y.-Y.; Shi, Q.-Z.; Zhu, Z. *Inorg. Chem.* **2013**, *52*, 14018–14027.
- (23) (a) Allman, T.; Goel, R. C.; Jha, N. K.; Beauchamp, A. L. *Inorg. Chem.* **1984**, *23*, 914–917. (b) Li, S. L.; Mak, T. C. W. *J. Chem. Soc., Dalton Trans.* **1995**, 1519–1530. (c) Wen, Y.-H.; Feng, X.; Feng, Y.-L.; Lan, Y.-Z.; Yao, Y.-G. *Inorg. Chem. Commun.* **2008**, *11*, 659–661. (d) Yang, Y.-Q.; Li, C.-H.; Li, W.; Kuang, Y.-F. *Chin. J. Inorg. Chem.* **2010**, *26*, 1890–1894. (e) Burrows, A. D.; Frost, C.; Kandiah, G. M.; Keenan, L. L.; Mahon, M. F.; Savarese, T. L.; Warren, J. E. *Inorg. Chim. Acta* **2011**, *366*, 303–309. (f) Zhang, Z.; Gao, W.-Y.; Wojtas, L.; Ma, S.; Eddaoudi, M.; Zaworotko, M. J. *Angew. Chem., Int. Ed.* **2012**, *51*, 9330–9334. (g) Wu, G.-Y.; Ren, Y.-X.; Yin, Z.; Sun, F.; Zeng, M.-H.; Kurmoo, M. *RSC Adv.* **2014**, *4*, 24183–24188. (h) Haldar, R.; Reddy, S. K.; Suresh, V. M.; Mohapatra, S.; Balasubramanian, S.; Maji, T. K. *Chem. - Eur. J.* **2014**, *20*, 4347–4356.
- (24) Hou, L.; Shi, W.-J.; Wang, Y.-Y.; Guo, Y.; Jin, C.; Shi, Q.-Z. *Chem. Commun.* **2011**, *47*, 5464–5466.
- (25) (a) Sun, D.; Ma, S.; Ke, Y.; Collins, D. J.; Zhou, H.-C. *J. Am. Chem. Soc.* **2006**, *128*, 3896–3897. (b) Klein, N.; Senkovska, I.; Gedrich, K.; Stoock, U.; Henschel, A.; Mueller, U.; Kaskel, S. *Angew. Chem., Int. Ed.* **2009**, *48*, 9954–9957. (c) Wang, Z.; Tanabe, K. K.; Cohen, S. M. *Chem. - Eur. J.* **2010**, *16*, 212–217. (d) Lee, Y.; Moon, H. R.; Cheon, Y. E.; Suh, M. P. *Angew. Chem., Int. Ed.* **2008**, *47*, 7741–7745.
- (26) Liao, P.-Q.; Zhou, D.-D.; Zhu, A.-X.; Jiang, L.; Lin, R.-B.; Zhang, J.-P.; Chen, X.-M. *J. Am. Chem. Soc.* **2012**, *134*, 17380–17383.
- (27) (a) Gao, W.-Y.; Pham, T.; Forrest, K. A.; Space, B.; Wojtas, L.; Chen, Y.-S.; Ma, S. *Chem. Commun.* **2015**, *51*, 9636–9639. (b) Seth, S.; Savitha, G.; Moorthy, J. N. *Inorg. Chem.* **2015**, *54*, 6829–6835. (c) Li, P.-Z.; Wang, X.-J.; Liu, J.; Lim, J. S.; Zou, R.; Zhao, Y. *J. Am. Chem. Soc.* **2016**, *138*, 2142–2145.
- (28) Myers, A. L.; Prausnitz, J. M. *AIChE J.* **1965**, *11*, 121.
- (29) Xiang, Z.; Peng, X.; Cheng, X.; Li, X.; Cao, D. *J. Phys. Chem. C* **2011**, *115*, 19864–19871.
- (30) (a) Nugent, P. S.; Rhodus, V. L.; Pham, T.; Forrest, K.; Wojtas, L.; Space, B.; Zaworotko, M. J. *J. Am. Chem. Soc.* **2013**, *135*, 10950–10953. (b) Liu, K.; Li, B.; Li, Y.; Li, X.; Yang, F.; Zeng, G.; Peng, Y.; Zhang, Z.; Li, G.; Shi, Z.; Feng, S.; Song, D. *Chem. Commun.* **2014**, *50*, 5031–5033.
- (31) Liu, B.; Jiang, Y.-H.; Li, Z.-S.; Hou, L.; Wang, Y.-Y. *Inorg. Chem. Front.* **2015**, *2*, 550–557.
- (32) Wen, H.-M.; Li, B.; Wang, H.; Krishna, R.; Chen, B. *Chem. Commun.* **2016**, *52*, 1166–1169.
- (33) (a) Haldar, R.; Reddy, S. K.; Suresh, V. M.; Mohapatra, S.; Balasubramanian, S.; Maji, T. K. *Chem. - Eur. J.* **2014**, *20*, 4347–4356. (b) Wang, H.-H.; Jia, L.-N.; Hou, L.; Shi, W.-J.; Zhu, Z.; Wang, Y.-Y. *Inorg. Chem.* **2015**, *54*, 1841–1846. (c) Wang, H.-H.; Shi, W.-J.; Hou, L.; Li, G.-P.; Zhu, Z.; Wang, Y.-Y. *Chem. - Eur. J.* **2015**, *21*, 16525–16531.